nature sustainability

SUPPLEMENTARY INFORMATION

https://doi.org/10.1038/s41893-019-0445-5

In the format provided by the authors and unedited.

Enhanced solar evaporation using a photo-thermal umbrella for wastewater management

Akanksha K. Menon[1,3], Iwan Haechler[1,3], Sumanjeet Kaur[1], Sean Lubner[1] and Ravi S. Prasher[1,2*]

[1]Energy Storage and Distributed Resources Division, Lawrence Berkeley National Laboratory, Berkeley, CA, USA. [2]Department of Mechanical Engineering, University of California, Berkeley, Berkeley, CA, USA. [3]These authors contributed equally: Akanksha K. Menon, Iwan Haechler. *e-mail: rsprasher@lbl.gov

Supplementary Information

Enhanced solar evaporation using a photo-thermal umbrella for wastewater management

Akanksha K. Menon[1$], Iwan Haechler[1$], Sumanjeet Kaur[1], Sean Lubner[1] and Ravi S. Prasher[1,2*]

[1] Energy Storage & Distributed Resources Division, Lawrence Berkeley National Laboratory, Berkeley, CA 94720, USA

[2] Department of Mechanical Engineering, University of California, Berkeley, CA 94720, USA

[*] Correspondence to rsprasher@lbl.gov

[$] Denotes equal contributions

Supplementary Note 1 – Radiative heat localization in water

The absorption of electromagnetic waves (and thus light) in matter is defined by the optical properties of the material through which the wave is travelling. With Beer-Lambert-Bouguer's law, the intensity of the incident wave at a given depth x can be determined as:

$$I(x) = I_0 e^{-\kappa x}$$

where I_0 is the incident intensity on the surface of the material, x is the distance from the surface (optical path length) and κ is the extinction coefficient. The extinction coefficient is a function of the material properties and also depends on the wavelength of incoming radiation.[1] Specifically, by using a UV-Vis and FTIR spectrometer, the transmittance of light through a medium can be measured as $\tau = I(x)/I_0$. Since water is a pure substance with no scattering, the extinction coefficient can be simplified to the absorption coefficient. For wavelengths between 250 – 800 nm (which comprises 60% of incoming sunlight), the absorption coefficient is very small ~ 0.01 m^{-1} and water acts as a transparent medium. However, at wavelengths larger than 2 µm (infrared), the absorption coefficient of water increases by nearly six orders of magnitude. Consequently, the penetration depth (inverse of the absorption coefficient, $1/\kappa$) of radiation decreases by several orders of magnitude, and heat is localized at the surface, thereby increasing the temperature where water evaporation occurs. Predominantly mid-IR emission is achieved using a blackbody with temperature, T < 150 °C. In this case, ~99.9% of thermal radiation lies at wavelengths above 2 µm, of which 90-95% is absorbed within microns of water as shown in Supplementary Fig. 2.

Supplementary Note 2 – Optical characterization of the solar umbrella

The optical properties of the selective solar absorber and black paint emitter were measured using an FTIR (Thermo Electron Nicolet 5700), coupled with an integrating sphere accessory (Pike Technologies Mid-IR IntegratIR). As the samples were non-transmitting, the absorptance was calculated as unity minus reflectance values shown in Supplementary Fig. 3.

Supplementary Note 3 – Lab-scale experimental testing

For lab-scale prototype testing, a solar simulator (Newport, 94081A) with an optical filter for AM 1.5G spectrum is used as the solar input. A power meter and thermopile detector (Newport, 919P-030-18) were used to measure the incoming solar flux at the same location as the water tank. The tank is made out of acrylic and comprises an inner pocket (square cross-section with a side length of 35 mm and a 5 mm depth) that is coated in a reflective foil and filled with water (to reflect radiation on the tank walls into water which provides a better representation of a large water body absorbing radiation) as shown in Supplementary Fig. 4. The inner pocket is surrounded by a 20 mm thick acrylic wall on all sides that minimizes thermal losses from the sides of the tank. Two K-type thermocouples were placed in the tank: one ~2 mm below the water surface to record the surface temperature, T_s, and one at the bottom of the inner pocket to record the bulk water temperature, T_b. The selective absorber-black emitter was mounted on Teflon spacers and placed ~3-4 mm above the water surface to maintain a large view factor for radiation. In this setup, the air gap between the hot emitter and cooler water surface acts as an insulting layer, thereby eliminating the need for an insulating foam. Another K-type thermocouple was attached to the surface of the emitter to measure its temperature, T_{abs}, and estimate the blackbody emissive power. A convective cover made of bubble wrap was placed on top of the absorber to reduce convection losses from the surface, and holes were made in it and in the absorber (covering less than 1% of its area) to allow vapor transport to the ambient. The tank was placed on a balance (A&D, GF-4000) that records the mass loss due to evaporation over time. A hygrometer (Onset, HOBO UX100) was kept next to the balance to measure ambient conditions (temperature, T_∞, and relative humidity). The K-type thermocouples were connected to a data logger (Pico Technologies, USB TC-08) that records temperature as a function of time. A 35 mm copper aperture was placed above the absorber to limit extraneous light from the solar simulator during experimental testing. As a first step, evaporation under dark conditions was measured for 30 minutes (solar simulator on with the shutter closed). Next, the shutter was opened with the incident flux set to 1000 W m^{-2}, unless otherwise noted. Mass loss and temperature measurements were made for two hours under illumination, and values reported in the manuscript are averaged over four runs with the dark evaporation subtracted. Limitations of this prototype include a view factor less than unity (~0.85), hindered vapor transport due to closeness of umbrella to water surface, and convection losses from the top surface of the absorber even with a convective cover.

Upon illumination, the selective absorber shows a rapid response for conversion of solar energy into heat. Under a solar flux of 1000 W m^{-2}, the absorber reaches a peak operating temperature of 70 ± 2 °C in ~ three minutes owing to the use of a high thermal conductivity substrate (aluminum in this case) and negligible re-radiation losses. Supplementary Fig. 5 also shows the water evaporation rate under dark conditions, under direct illumination corresponding to volumetric heating, and using the solar umbrella corresponding to surface heating.

The lab-scale prototype was tested at different optical concentrations of 1, 3 and 5 suns. As expected, at higher solar fluxes, the absorber-emitter temperature increases, which in turn results in a higher emissive power on the water, thereby increasing the surface temperature. As an illustration, at 5000 W m^{-2}, the evaporation rate increases to 1.6 kg m^{-2} h^{-1} as the water surface temperature is 60 °C in one hour while the bulk remains at 30 °C, as shown in Supplementary Fig. 6. The absorber-emitter can also be used for generating hot vapor as the evaporated water quickly mixes with the air surrounding the hot absorber. A thermocouple was placed 2 mm below the absorber surface to measure the vapor temperature as it escapes from the holes. Significantly higher absorber temperatures can be achieved using a convective cover or an evacuated plate that eliminates convection losses from the hot absorber. Non-tracking wide-angle optical concentrators can provide a passive and cost-effective approach to concentrate sunlight for evaporation.

Brine evaporation experiments: Continuous evaporation from a saturated brine solution (25 wt% NaCl in water) under natural sunlight no visible contamination or salt deposition on the emitter surface even after several days of operation, as shown in Supplementary Fig. 7. This confirms that the solar umbrella can be used as a fouling-resistant device for brine concentration towards achieving zero-liquid discharge.

Supplementary Note 4 – Heat and mass transfer model

The overall system comprises two main sub-systems as shown in Supplementary Fig. 8: the solar umbrella (absorber and emitter) and the water tank. The umbrella receives incoming solar flux (Q_{solar}), and absorbs a majority of it owing to a high solar absorptance of 0.95. As its temperature increases, 5% losses by thermal radiation (Q_{rad}) as well as convection losses at the top surface (Q_{conv}) occur to the ambient. Since the absorber and emitter coatings are thin layers on an aluminum substrate, the structure is isothermal, and the emitter radiates in the IR (Q_{emit}) to the water surface. Performing an energy balance on the umbrella,

$$Q_{solar} = Q_{conv} + Q_{rad} + Q_{emit}$$

Performing an energy balance on the water surface:

$$Q_{emit} = Q_{conv,w} + Q_{rad,w} + Q_{cond} + Q_{evap}$$

where $Q_{rad,w}$ and $Q_{conv,w}$ are the radiation and convection losses from water respectively (tank walls + water surface), Q_{cond} is the conduction losses from the surface to the underlying bulk water and Q_{evap} is the remaining energy that is available for evaporation. Here:

$$Q_{rad,w} = F\varepsilon\sigma(T^4 - T_\infty^4)$$

$$Q_{conv,w} = h_{conv}(T - T_\infty)$$

$$Q_{cond} = -k\left(\frac{T_s - T_b}{L}\right)$$

$$Q_{evap} = \dot{m}h_{fg} = h_{evap}(T_s - T_\infty)$$

where F is the view factor, ε is the emittance, T is the temperature of the surface, T_∞ is the ambient temperature, h_{conv} is the convective heat transfer coefficient, k is the thermal conductivity of water, T_s is the water surface temperature, T_b is the bulk water temperature and h_{evap} is the evaporation heat transfer coefficient. h_{evap} is calculated as an average value using T_s and $\dot{m}$ data at different optical concentrations shown in Supplementary Fig. 6 to obtain a value of 28 W m^{-2} K^{-1}. The water tank can be treated as a horizontal rectangular cavity with a heated top surface since radiative heat localization results in a higher temperature at the water surface compared to the bulk. In this configuration, convection within the volume of water is neglected as heat transfer within the enclosed fluid is exclusively by conduction (in the absence of radiation) for all values of Rayleigh numbers.[2]

In the lab-scale prototype, due to the large view factor between the umbrella and water surface and the small gap, radiation emitted by the water surface is largely absorbed by the emitter, which in turn emits back to the water surface. As a result, less than 1% radiation loss occurs between the water surface and ambient. However, the walls of the water tank exchange radiation with the ambient and experience convection as well, both of which constitute thermal losses.

Heat transfer in the gap between the emitter and water in the lab-scale prototype is dominated by radiation between the two surfaces due to its non-contact nature. Convection losses in the quiescent gap are absent since the hot emitter (T_{abs}) is placed above the cold water surface (T_s); in this configuration the fluid density increases in the direction of the gravitational force and creates a stable temperature gradient without bulk fluid motion.[2] As a result, heat transfer is by conduction, which is small (~14% based on the validated thermal model) compared to the radiation exchange between the emitter and water surfaces. However, as evaporation occurs from the water surface, there is an upward flow of vapor (advection) that can reduce conduction in the lab-scale prototype gap of thickness L = 4 mm. To evaluate the effect of this flowing vapor on heat transfer in the quiescent gap, the Rayleigh number, Ra_m is calculated accounting for density differences caused by both temperature and concentration gradients:

$$Ra_m = Gr \times Sc = \frac{g(\Delta\rho/\rho)L^3}{\upsilon D_{AB}} = 128$$

where Gr is the Grashof number, Sc is the Schmidt number, g is the gravitational constant, $\Delta\rho$ is the density gradient accounting for both air and water vapor in the gap, $\rho$is the average density of the mixture, υ is the kinematic viscosity of air, and $D_{AB}$is the binary diffusion coefficient of water vapor and air. This is an order of magnitude lower than the critical value of 1708, only above which advection occurs.[2] Hence, non-radiative heat transfer in the gap is purely by conduction, which itself is only 14% of the heat transfer between the surfaces, and there are no convection losses between the emitter and water surfaces.

For a practical application of a solar umbrella on a large area evaporation pond, the distance of the emitter from the water surface, L must be small compared to the lateral dimensions of the pond (side length, X) for efficient radiation heat transfer. Treating the umbrella and pond as aligned parallel squares exchanging radiation, the view factor can be computed as:[2]

$$F = \frac{2}{\pi \bar{X}^2}\left\{\ln\left[\frac{(1+\bar{X}^2)^2}{1+2\bar{X}^2}\right]^{0.5} + \left(2\bar{X}(1+\bar{X}^2)^{0.5}\tan^{-1}\frac{\bar{X}}{(1+\bar{X}^2)^{0.5}}\right) - 2\bar{X}\tan^{-1}\bar{X}\right\}$$

where $\bar{X} = \frac{X}{L}$. This equation is plotted in Supplementary Fig. 9 and shows that for a view factor above 0.8, the umbrella should be placed above the pond such that $L \leq 0.1\ X$. This means that for a real pond where X is ~10 m or larger,[3] L can be as large as 1 m while maintaining a view factor above 0.8, indicating that most of the radiation leaving the emitter is incident on the pond surface. In this case, $Ra \sim 10^9$ and advection from the flowing vapor can ultimately eliminate conduction in the gap such that heat transfer between the emitter and water surfaces is by radiation alone, *i.e.,* the overall heat transfer between the umbrella and the pond will be reduced by ~14% as compared to the lab-scale prototype. To capture this realistic case, the COMSOL model predictions for a real evaporation pond are based only on radiation heat transfer between the emitter and water surface, and any effects from gap conduction that is specific only to the small-scale lab setup are excluded. Furthermore, this model includes convection losses from the water surface to the ambient air by assuming a heat transfer coefficient of 5 W m^{-2} K^{-1}, which is small compared to the effective heat transfer coefficient due to evaporation (28 W m^{-2} K^{-1}).

Mass transfer from the water surface to the ambient occurs by vapor formation at the liquid-vapor interface and vapor transport from the surface into the ambient. The first step is represented by a kinetic resistance, R_0 (see Supplementary Fig. 10) that can be calculated using the Hertz-Knudsen equation[4] for evaporation:

$$\dot{m} = \sqrt{\frac{M_w}{2\pi R T_s}}\sigma_e P_{sat}(T_s)$$

For T_s = 42 °C obtained with the solar umbrella under one sun, $\dot{m}$ calculated using this equation is significantly higher than the experimentally measured mass flux (10 kg m^{-2} s^{-1} vs. 0.01 kg m^{-2} s^{-1}). Therefore liquid-vapor interface mass transport resistance can be neglected, *i.e.,* $R_0 \sim 0$, indicating that mass transfer in the system is not phase change-limited. In the next step, vapor transport from the water surface to ambient is controlled by density differences arising from both temperature and concentration gradients. Since water evaporation in air at temperatures below boiling constitutes a dilute species mixture, the heat and mass transfer analogy[2] can be used to predict the mass transfer coefficient (comprising diffusion and advection) and evaporation rate, $\dot{m}$ as a function of device geometry and flow conditions:

- <u>Lab-scale device</u>: Mass transport resistance of the gap between the water surface and emitter, R_1 is dominated by diffusion; this is supported by the small value of mass transport Rayleigh number (Ra_m) obtained by modeling the confined gap as a rectangular cavity with a characteristic length scale of L = 4 mm as shown in Supplementary Fig. 10a. Correlations for natural convection yield Ra_m <1708, which is the critical value beyond which advection effects become important,[2] which in this case occurs only for L ~1 cm. As a result, there is no advection and the lab-scale setup is diffusion-limited. Thus, evaporation in the lab-scale device is hindered by the closeness of umbrella to water surface, which results in a higher humidity and temperature in the gap, both of which adversely impact mass transport. The evaporation rate is mainly controlled by the vapor diffusion rate with a mass transfer coefficient h_m = 0.0042 m s^{-1}; this is in agreement with various literature reports on evaporation and solar steam generation devices, which are also diffusion-limited.[5,6]

- Large-area evaporation pond: A real evaporation pond can have length > 10 m such that the umbrella can be placed as far away as 1 m while maintaining a radiation view factor >0.8 (Supplementary Fig. 9). As a result, the gap between the emitter and water surface is no longer confined and mass transfer can be modeled with a single resistance, R_3 as a heated horizontal flat plate with a characteristic length $L = A_s/P$ for natural convection. As a limiting case, evaporation into quiescent air, *i.e.*, natural convection only is considered, which yields $Ra_m > 10^9$ indicating that advection will dominate and enhance evaporation from the pond. The mass transport boundary layer thickness for natural convection is calculated as ~5 cm using the heat and mass transfer analogy. Therefore, holes are no longer required since the distance between the umbrella and water surface is larger than the boundary layer, implying that ambient conditions exist in the gap as shown in Supplementary Fig. 10b.

This analysis indicates that the lab-scale device performance represents a lower bound, which is expected to improve in a real application where the gap has ambient conditions and surface area is five orders-of-magnitude larger. Furthermore with external wind for a real pond, evaporation rate can increase due to forced convection. Therefore, estimates for evaporation from a real pond (Figure 5a of the manuscript) are conservative because the mass transfer coefficient applied to the pond is the same as the diffusion-limited lab-scale prototype (h_m = 0.0042 m s^{-1}). For a real pond in which the distance between the umbrella and the water surface can be very large (compared to the boundary layer thickness), advection enhances h_m to 0.009 m s^{-1}, resulting in an evaporation rate of 1.4 kg m^{-2} h^{-1}.

Supplementary Note 5 – COMSOL thermal model

The lab-scale setup is modeled using COMSOL Multiphysics software and thermal losses are estimated. Water in the acrylic tank is modeled with the following boundary conditions: convection on all side walls = 5 W m^{-2} K^{-1}, radiation from all side walls and water surface with emissivity = 0.95, thermal insulation on bottom surface, evaporation coefficient of 28 W m^{-2} K^{-1} on water surface and a boundary heat flux of 680 W/m^2 on the water surface (this corresponds to the radiation from the emitter at 72 °C under 1 sun accounting for its emissivity and the view factor). The initial water temperature is set at 22.5 °C and the ambient temperature is 25 °C. Spectral radiation in participating media is used to model the high absorption coefficient of water in mid-IR (peak wavelength ~8 μm with absorption coefficient 10^4 m^{-1}), resulting in heat localization at the surface. The absorber is modeled with a spectrally selective emissivity (absorptance of 0.95 for solar wavelengths and thermal emittance of 0.04 at wavelengths larger than 2.5 μm). The black paint emitter surface is modeled with an emittance of 0.94.

For evaporation pond simulations, the geometry is modified to a surface with 1 m radius and a 0.5 m depth as shown in Supplementary Fig. 11. Owing to the large surface area, convection and radiation losses from the sides of the system are negligible compared to the lab-scale prototype. Furthermore, for a large pond, the view factor between the umbrella and water surface is 1 (*i.e.,* all the radiation leaving the umbrella is intercepted by the water surface) so a boundary heat flux of 750 W m^{-2} is used at the water surface.

Supplementary Note 6 – Comparison of surface and bulk heating

Given the diurnal and intermittent nature of sunlight, a small thermal mass is desirable so as to reduce the transient heating time of the water surface. In other words, water surface temperature should increase rapidly with solar illumination, thereby minimizing the time lag for water evaporation. Using the solar umbrella, sunlight is converted into infrared radiation which is absorbed within a 100 μm layer of water. Since this is a small thermal mass, the transient heating time is small and T_s increases to over 40 °C within one hour in the lab-scale prototype and outdoor experiments. In comparison, without the umbrella, solar energy is used for sensible heating of the entire volume of water which has a higher thermal mass, resulting in a temperature increase to only 27 °C in the same one hour period. The transient response for both cases (with and without the solar umbrella) is shown in Supplementary Fig. 12a and confirms that the time taken is much smaller when heat is localized at the surface, thereby minimizing the time lag for evaporation.

To evaluate when bulk heating can achieve temperatures comparable to surface heating, we investigate the effect of water depth on surface temperature with two cases: *(i)* bulk heating in an evaporation pond with a black-coated floor, and *(ii)* interfacial heating in an evaporation pond with a solar umbrella are compared. For the bulk heating case, solar energy is absorbed at the bottom (black-coated floor) and transferred upward to the water surface by conduction and convection through the depth of the pond. In contrast, the solar umbrella localizes heat within 100 μm of the water surface irrespective of pond depth due to its strong infrared absorption. The validated thermal model is used to compare the surface temperatures attained in one hour for both these cases; Supplementary Fig. 12b shows that bulk heating will become comparable to surface heating only if the pond depth (or water thickness) is smaller than 1 cm. Given that large area evaporation ponds have typical depths ranging from 0.5 to 2 m,[3] adding a solar umbrella result in a performance enhancement by increasing water surface temperature, which in turn increases the evaporation rate and the solar-thermal efficiency.

Supplementary Note 7 – Literature comparison

During the review process for this manuscript, we became aware of the non-contact solar steam generation device proposed by Cooper et al.[7] In this section, we provide a detailed comparison between their concept and the solar umbrella proposed in this paper:

- Application: The contactless solar evaporation structure (CSES) targets high temperature steam generation (>120 °C) for sterilization and process heat.[7] The solar umbrella targets increased mass flux from large area evaporation ponds with a simple design for desalination and ZLD, in which case evaporation rate is more important than temperature.
- Design and performance: For evaporation ponds, the key metric from a technological standpoint is the ratio of cost of the device and mass flux. With this in mind, we have proposed a simple design (comprising a selective solar absorber used in domestic hot water heaters, a spray on black paint with high emissivity used in furnaces, and a plastic sheet as a convective cover) that minimizes device cost while maintaining a high mass flux. Supplementary Table 1 summarizes the differences between the two prototypes under 1 sun operating conditions.

For ZLD applications under one sun where evaporation rate (mass flux) or solar-thermal efficiency is the most important parameter, Table S1 shows that the performance of the solar umbrella is 70% better than the CSES. Furthermore, the solar umbrella was tested for salt concentrations up to 25 wt% (saturation condition for NaCl in water) which is much more applicable for ZLD, whereas the CSES was tested only up to 3.5% (seawater). This is important since salt concentration has an effect on evaporation rate as vapor pressure decreases with increasing salinity, thereby reducing the driving force for evaporation. The CSES uses a triple-layer glazing to minimize convective losses from the absorber, leading to temperatures >120 ^{o}C for superheated steam generation. This, along with the use of a superheater (aluminum shell with a carbon foam) is used to obtain a vapor temperature of 122 °C, albeit at the cost of a reduced efficiency of 25%.[7] In contrast, since the solar umbrella is targeted to be a low cost solution for enhancing mass flux, bubble wrap is used to reduce convection losses and maintains the emitter at 72 °C. As a result, the vapor reaches a temperature 66 ^{o}C when it leaves the holes in the emitter, and a higher efficiency of 43% is achieved. If desired, the emitter temperature can be increased by insulating the surface in order to generate high temperature vapor or steam. For water desalination and ZLD application, increased mass flux and design simplicity for reduced capital cost of device or system are key, and these have been the guiding metrics for designing the umbrella. Therefore, the CSES is more suitable for applications such as sterilization and process heating, while the umbrella is tailored for ZLD and desalination.

- Scalability and cost of produced water or solid waste: The cost of produced water in the case of desalination (or cost of produced waste in the case for ZLD) is proportional to: $capital\ cost\ of\ device/\ mass\ flux$ [$/LMH]. The CSES design consists of numerous components and multiple insulation layers including aerogel (see Supplementary Note 6 in reference [7]) that are required in order to achieve high temperature steam. In contrast, the solar umbrella comprises a spectrally selective solar absorber on a metal substrate, with a spray-on black paint coating on the bottom and a bubble wrap convection shield. This simple design lends itself to large area applications such as evaporation ponds as it is scalable. As such, the capital cost of the solar umbrella will be significantly lower than the CSES, and since the mass flux is also higher, the $/LMH value is projected to be low.

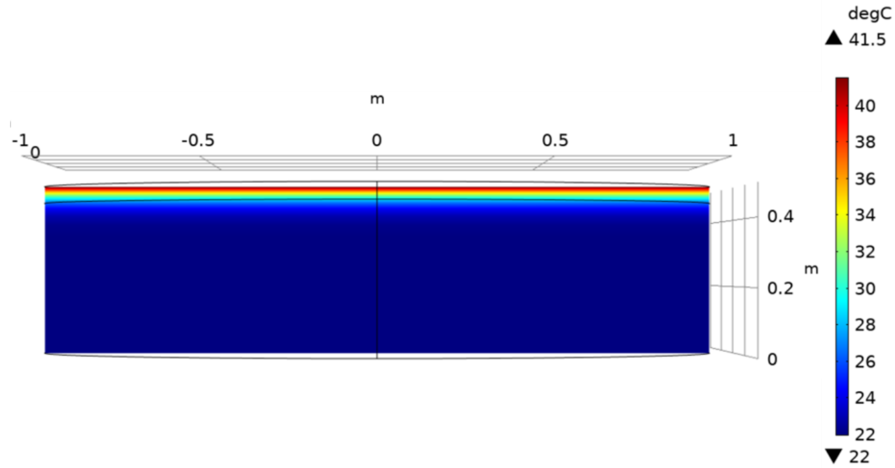

Supplementary Figure 1. COMSOL simulation of an evaporation pond. The color bar shows heat localization at the surface when using a photo-thermal umbrella, resulting in an enhancement in evaporation rate under one sun.

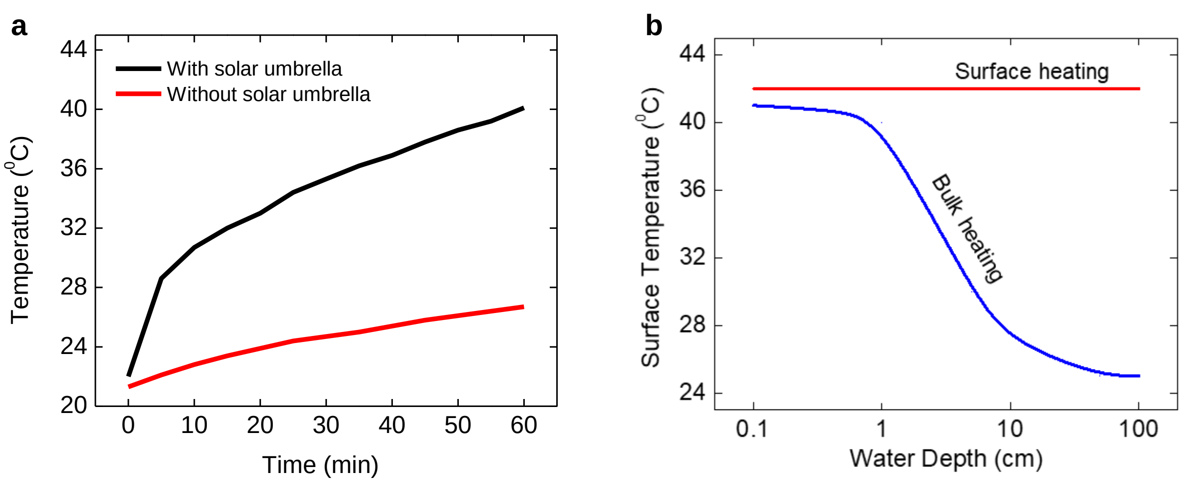

Supplementary Figure 2. Comparison of surface and bulk heating. (a) Transient heating profiles for surface heating (with solar umbrella) and bulk heating (without solar umbrella) show that a higher temperature is attained in a shorter amount of time with surface heating. **(b)** Temperature of the water surface as a function of evaporation pond depth for bulk heating and surface heating.

Supplementary Table 1. Summary of parameters for radiative heat localization prototypes

	CSES (Cooper et al.[7])	**Solar umbrella (this work)**
Solar-thermal efficiency (%)	24.6	43
Mass flux (kg m^{-2} h^{-1})	0.39	0.62
Salt concentration tested (NaCl wt%)	3.5	25 (saturation limit)
Temperature of emitter (ºC)	124	72
Temperature of vapor (ºC)	122	62
Target applications listed	Sterilization, autoclaving, cooking, process heat, solar distillation	Evaporation ponds for ZLD, desalination

Supplementary References

1 Segelstein, D. J. *The complex refractive index of water*, University of Missouri-Kansas City, (1981).

2 Incropera, F. P. *Fundamentals of heat and mass transfer*. (John Wiley, 2007).

3 Principles of Design and Operations of Wastewater Treatment Pond Systems for Plant Operators, Engineers, and Managers. (2011).

4 Persad, A. H. & Ward, C. A. Expressions for the Evaporation and Condensation Coefficients in the Hertz-Knudsen Relation. *Chemical Reviews* **116**, 7727-7767, doi:10.1021/acs.chemrev.5b00511 (2016).

5 Lu, Z., Kinefuchi, I., Wilke, K. L., Vaartstra, G. & Wang, E. N. A unified relationship for evaporation kinetics at low Mach numbers. *Nature Communications* **10**, 2368, doi:10.1038/s41467-019-10209-w (2019).

6 Ni, G. *et al.* Steam generation under one sun enabled by a floating structure with thermal concentration. *Nature Energy* **1**, 16126, doi:10.1038/nenergy.2016.126

https://www.nature.com/articles/nenergy2016126#supplementary-information (2016).

7 Cooper, T. A. *et al.* Contactless steam generation and superheating under one sun illumination. *Nature Communications* **9**, 5086, doi:10.1038/s41467-018-07494-2 (2018).